

Experimental Assessment of Seismic Vulnerability of Corner Beam-Column Joints in Older Concrete Buildings

Wael M. Hassan

Ph.D., P.E. S.E Skidmore, Owings & Merrill LLP, San Francisco, CA, USA

Jack P. Moehle

Ph.D., P.E. University of California, Berkeley, CA, USA



15 WCEE
LISBOA 2012

SUMMARY

Older concrete beam-column joints that lack transverse reinforcement (unconfined joints) are susceptible to severe damage possibly contributing to building collapses during strong earthquakes. Tools to predict shear strength of joints with ductile details exist. In addition, many retrofit strategies for existing joints are available; however, tools to assess existing joint capacity are lacking. The current study aimed to improve seismic performance understanding of unconfined corner joints in existing buildings. Four full-scale, 3D, corner joint sub-assemblages, with slab, were tested under unidirectional and bidirectional cyclic loading varying axial loads to simulate overturning effects. The test parameters are axial load level, joint aspect ratio, loading history, and beam reinforcement. Test results showed the potential for early shear failure of unconfined joints. Two distinct joint failure modes were identified based on reinforcement ratio and joint aspect ratio. Joint shear strength varies inversely with aspect ratio. Axial load effect on shear strength and deformation capacity varies based on failure mode. Axial failure of joints appears to be unlikely within the practical drift limits. Elliptical shear strength interaction seems suitable for bidirectional loading. Tests revealed the inaccuracy of shear strength of existing building guidelines.

Keywords: beam-column joints, cyclic test, reinforced concrete, shear strength, transverse reinforcement, axial failure

1. INTRODUCTION

Inadequate corner joints are believed to have contributed to building collapses during past earthquakes. The seismic performance of interior and exterior unconfined beam-column joints has been investigated by several research studies. However, corner joints have received less attention despite apparent vulnerability. Moreover, in the few available corner joint tests, realistic building boundary conditions, concrete slab, and representative axial load level variation were absent. The current study is a part of the Network for Earthquake Engineering Simulation (NEES) Grand Challenge research project: Mitigation of Collapse Risk of Older Concrete Buildings. It aims to experimentally quantify the seismic vulnerability of older corner joints lacking transverse reinforcement by testing four full scale joint subassemblies with realistic loading and boundary conditions. Estimating the likelihood of joint axial failure following shear damage was a key goal of this study. Hassan et al. 2010 summarized the key parameters influencing joint strength and ductility and identified the various modes of failure of deficient joints.

2. EXPERIMENTAL PROGRAM

2.1. Test Objectives and Parameters

The main test objective was to better understand the seismic performance of unconfined corner beam-column joints by assessing the joint shear strength, deformation capacity, and residual axial capacity under different loading schemes and joint configuration. The main test parameters were beam reinforcement ratio, joint aspect ratio α_j (beam depth h_b to column depth h_c ratio), axial load ratio, and loading history. A major objective was to address the seismic vulnerability of shear-damaged joints to axial failure. The test was to serve as a basis for calibration and verification of joint shear strength and axial capacity models. Table 2.1 presents the test parameters.

2.2. Test Specimens Details and Instrumentation

Four full-scale, 3D, corner beam-column sub-assemblages, including slab, were modeled, Fig. 2.1. The test specimen represents the portion of a corner bay bounded by inflection points. No joint reinforcement was provided. Hassan et al. 2010 identifies different modes of unconfined joint failure. Two modes of inelastic response were of interest: J-Failure (joint shear failure occurs without beam or column yielding) and BJ-Failure (joint failure occurs following beam flexural yielding). Test specimens U-J-1, U-J-2, and B-J-1 were intended to have J-Failure, and specimen U-BJ-1 was intended to have BJ-Failure. The columns were made sufficiently strong that only mild or no yielding of columns was expected. The concrete strengths for specimens U-J-1, U-J-2, B-J-1, and U-BJ-1 were 4.3, 4.43, 4.41, and 4.39 ksi, respectively, while the average longitudinal and transverse reinforcement yield strengths were 74 ksi and 70 ksi, respectively. The test specimens were instrumented (Fig. 2.2) to measure the global response, local deformations, and strains using a total of 200 data channels per specimen. Steel strains at critical sections were measured using 60 strain gages per specimen. External instrumentation measured displacement along beam span, twisting rotation in beams and columns, shear and flexural beam and column deformations, joint shear strain, and test setup and specimen global displacements.

Table 2.1. Test matrix

Specimen ID	Loading History	α_j	Beam reinf. ratio		Axial load ratio		Failure mode
			ρ_t	ρ_b	Gravity	At shear failure	
U-J-1	Unidirectional	1	0.022	0.016	0.21	0.30	J
U-J-2	Unidirectional	1.67	0.010	0.007	0.21	0.45	J
B-J-1	Bidirectional	1	0.022	0.016	0.21	0.45	J
U-BJ-1	Unidirectional	1	0.009	0.007	0.21	0.45	BJ

2.3. Test Setup and Testing Protocol

The test setup is designed to mimic idealized structure boundary conditions. The setup boundary conditions satisfy moment releases at column ends through 3D universal hinges designed to accommodate high compression and tension forces and to allow free rotation. Vertical translation of the column is permitted to accommodate the expected shortening or elongation during intense overturning axial load reversals. Finally, horizontal translation and rotation of beams are permitted. The test setup (Fig. 2.3) consists of vertical axial loading system, lateral loading system, and lateral restraint system. The vertical axial loading system comprises two 360-kip capacity hydraulic actuators, with a total test setup capacity of 720 kips in axial compression and 360 kips in tension. The two actuators are connected to two horizontal W36 loading girders, which are sufficiently stiffened to resist local deformations. The loading girders are connected to the specimen through 3D universal hinges and transition plates. The lateral restraint system consists of the lateral frame of two HSS tube sections connected together with several HSS connectors and

a diagonal bracing member. Arrangements were made to allow vertical displacement of the vertical loading system including the specimen, by permitting its “frictionless” motion through the vents of the lateral frame. The lateral loading system consists of two vertical 120-kip capacity hydraulic actuators used to load the two orthogonal concrete beams bi-directionally, either simultaneously or in an alternating fashion.

To simulate gravity loading, the column is initially loaded monotonically with a gravity load of $0.21A_g f'_c$, while both beams are simultaneously displaced with initial offset downward displacement of $\Delta y/4$ to mimic floor gravity loading; where Δy is the beam theoretical yield displacement. Downward (pull-down) beam displacements are considered negative throughout this paper. Following simulated gravity loading, test specimens were subjected to a symmetric cyclic displacement pattern centered around the deformed gravity load position until collapse. Figure 2.4 displays test displacement histories. The displacements are commanded to beam actuators unidirectionally in two orthogonal directions in alternating fashion for specimens U-J-1, U-J-2, and U-BJ-1 or simultaneously commanded to both beams in the bidirectionally loaded specimen B-J-1. The relatively simple bidirectional 45-degree loading path is intended to simplify results interpretation. The axial load on a corner column during an earthquake could vary significantly due to overturning moment effects, ranging from tension to high compression. Once a building reaches a plastic state and thereafter, the axial load variation should continue at nearly the same amplitude provided that most of the building does not degrade. In specimen U-J-1, overturning effect was simulated by varying the column axial load as a linear function of beam shears. This resulted in excessive degradation of the axial force variation as the joint degraded. For specimens U-J-2, B-J-1 and U-BJ-1, the axial force protocol was changed so the axial force variation would be similar to that obtained when specimen strength was first achieved.

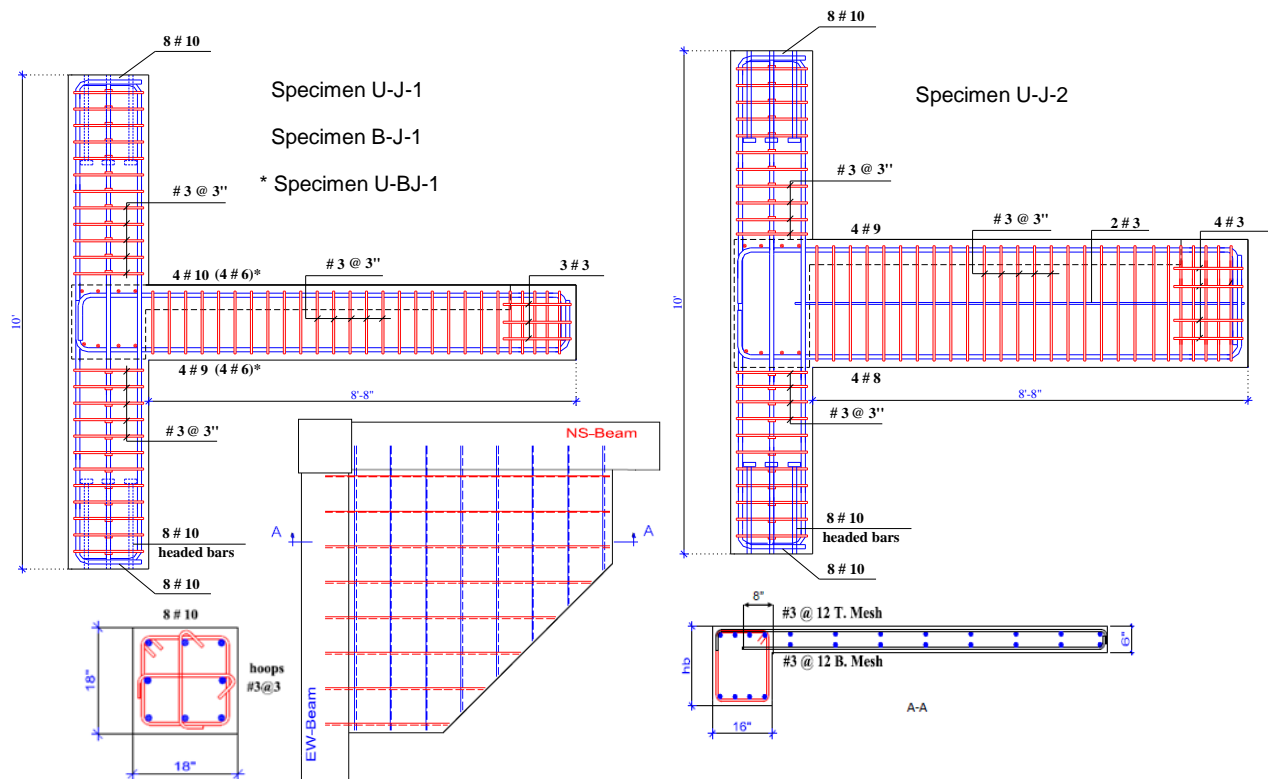


Figure 2.1. Test specimen details

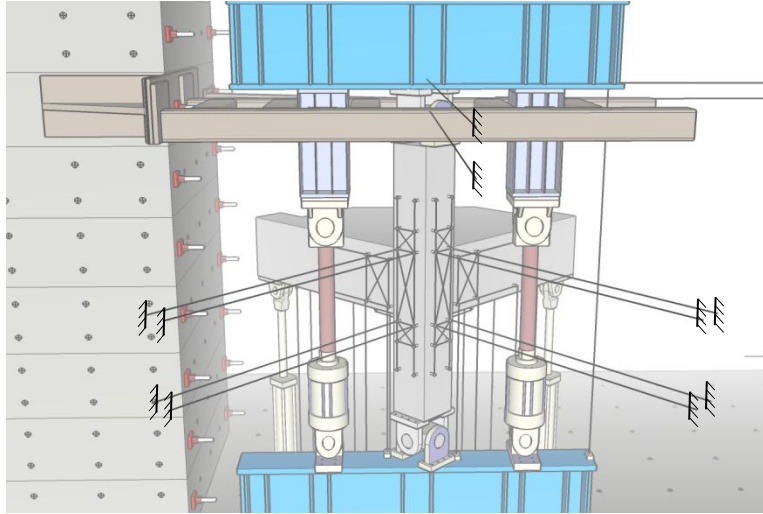


Figure 2.2. Specimen and test setup instrumentation

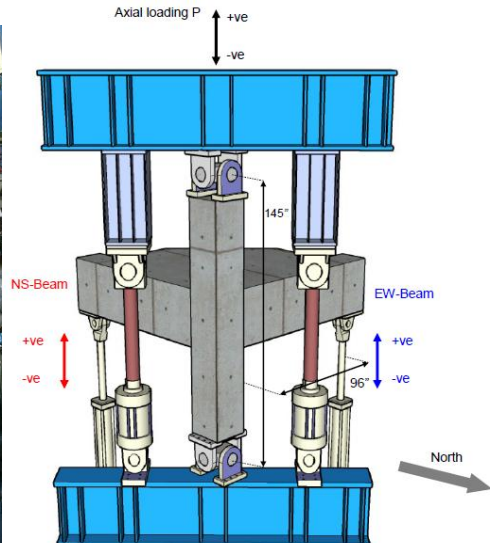
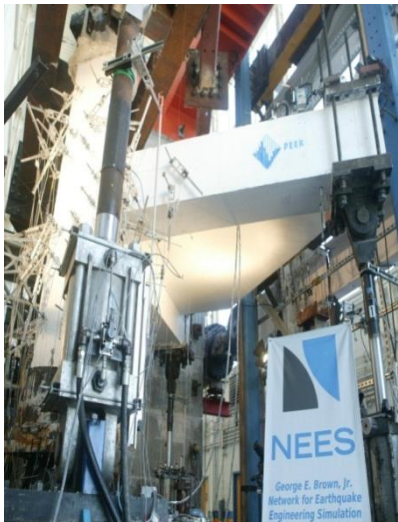


Figure 2.3. Test setup and loading pattern

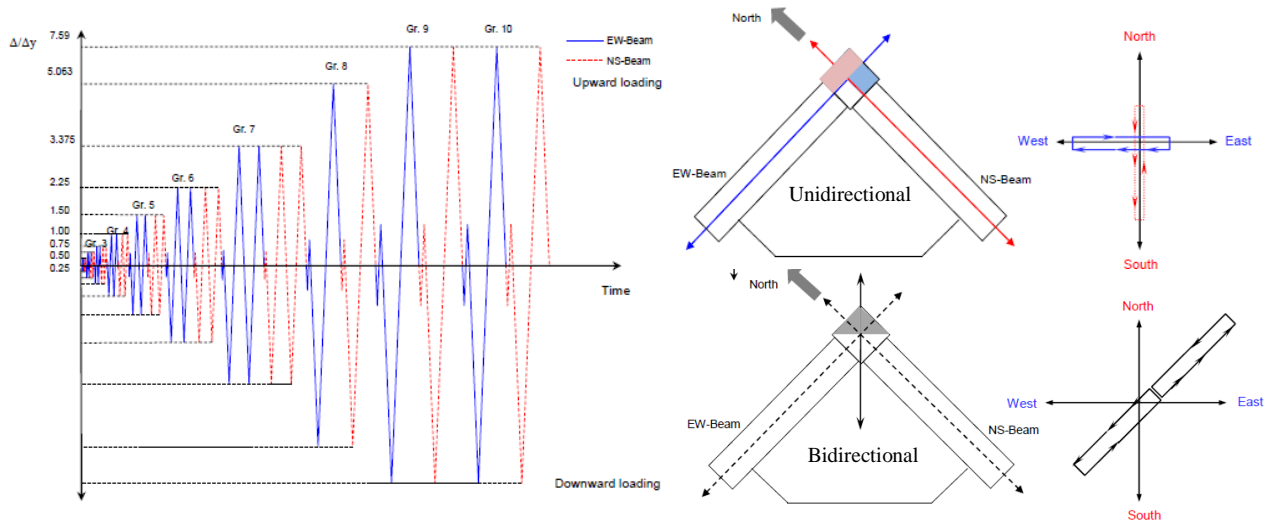


Figure 2.4. Lateral loading protocol

3. TEST RESULTS

3.1 Specimen U-J-1

This specimen experienced J-Failure mode at -2.19% EW downward drift. The joint shear strength coefficient γ_j , where joint shear strength is $V_n = \gamma_j A_j \sqrt{f'_c}$ psi, was 14.3 at an axial load ratio of 0.31. In this paper, the responses of EW beam loading only are shown. Beam reinforcement bar slip and hook prying were evident at large drifts. Figure 3.1 displays the force-drift ratio relations for the EW beam of specimen U-J-1. The pinched hysteresis loops due to joint inclined cracking are evident. Joint shear strength according to ASCE 41 2006 is low relative to measured strength. Figure 3.2 shows damage at development of joint strength. Figure 3.3 shows the joint area immediately prior and during axial failure. The joint suffered substantial shear damage before axial failure. Since the axial load level was relatively moderate, the specimen was able to survive large drifts before axial failure, which took place at -9.68% drift ratio. The residual axial load ratio was 20% at axial failure, while the residual shear strength was 20% of the peak strength. Figure 3.4 displays joint shear stress-strain backbone curves. The shear strain at downward loading peak strength was -0.0066 rad. Table 3.1 presents detailed test results of the specimen.

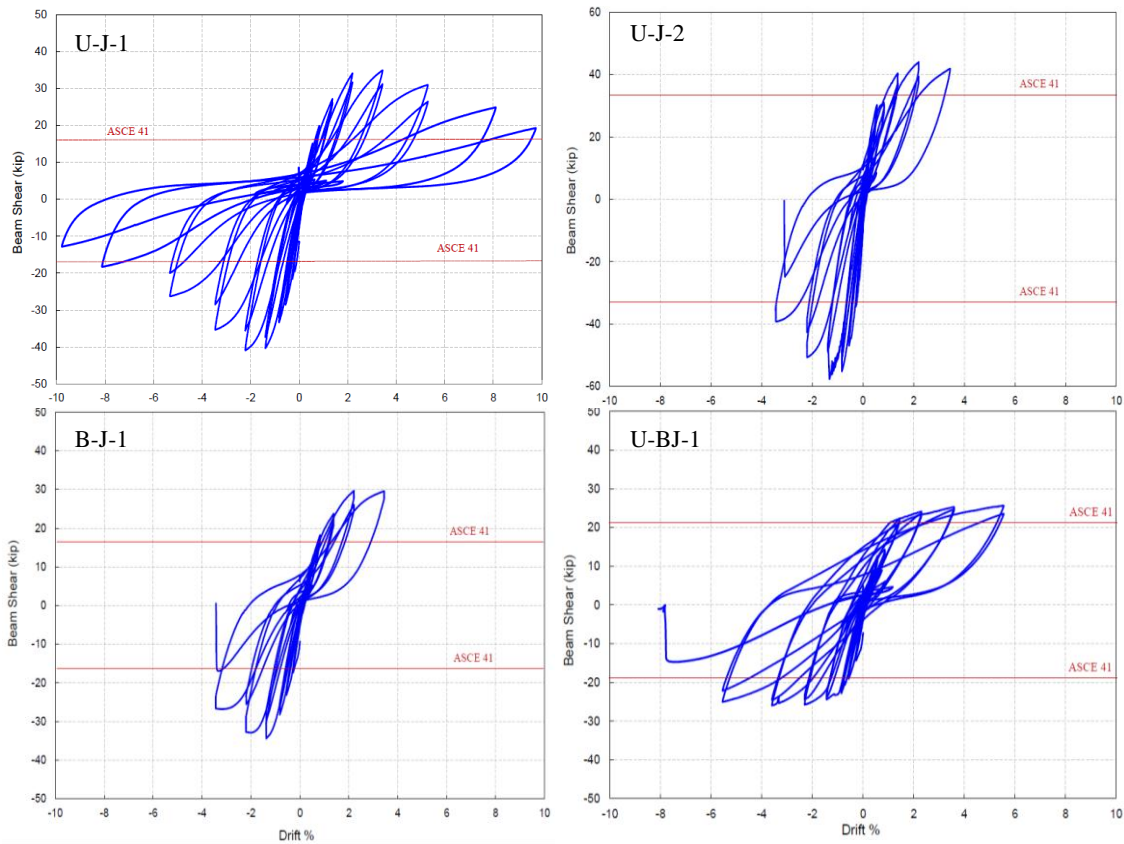


Figure 3.1. Beam shear force-drift hysteresis response of test specimens

3.2. Specimen U-J-2

In this specimen the first major diagonal crack occurred at EW $\pm 0.82\%$ drift ratio. The main diagonal crack extended above and below the joint toward the outermost side of the column. The specimen experienced a J-Failure mode (Fig. 3.3) at EW -1.30% drift and joint shear strength coefficient γ_j of 9.98 at an axial load ratio of 0.46. Figure 3.1 displays the shear force-drift ratio response of the EW beam loading of specimen U-J-2. The response is characterized by accelerated post-peak strength and stiffness degradation due to substantial axial load effect. It is evident that the joint shear strength estimation of

ASCE 41 is conservative for this specimen. Prior to axial failure, joint diagonal and vertical cracks significantly widened, and a significant bulging of joint concrete cover was observed, possibly caused by buckling of column longitudinal reinforcement within the joint. Unlike specimen U-J-1 with lower axial load, no joint concrete cover spalling occurred, hence the axial failure occurred relatively suddenly at -3.06% drift, Fig. 3.3. The axial load ratio was 0.43 at axial failure, while the residual lateral strength was 42% the peak shear strength. Figure 3.4 displays joint shear stress-strain backbone curves. The shear strain at downward loading peak strength was -0.0045 rad. Table 3.1 presents detailed test results of the specimen.

3.3. Specimen B-J-1

The first joint shear crack appeared at -0.82% drift. This specimen, which was bidirectionally loaded, experienced a J-Failure mode (Fig. 3.2) at 1.37% downward drift. The joint shear strength coefficient γ_j was 11.7 at an axial load ratio of 0.45. Joint shear cracking does not appear to follow diagonal pattern like unidirectional loading case due to the complex nature of stresses in bidirectional loading. The force-drift responses of EW and NS beams were almost identical. Figure 3.1 displays the force-drift ratio relations for the EW beam of specimen B-J-1. The post-peak hysteretic loops are distinctively different from those of unidirectional specimen; they appear to be wider and more pinched. The hysteresis loops exhibit more flexible response than that of specimen U-J-1 due to smaller column compression zone. The joint shear strength estimation of ASCE 41 is also conservative in the bidirectional loading case. The joint strain at peak shear strength was -0.0036. Axial failure (Fig. 3.3) took place at -3.36% drift ratio with a residual axial load ratio of 0.45 and residual shear strength of 50%.

3.4. Specimen U-BJ-1

In this BJ-Failure specimen, both EW and NS beams underwent significant yielding prior to joint shear failure. EW beam had first yield at -0.92% drift ratio with the first significant flexural crack occurring at -1.43% drift ratio. The force-displacement loops are wider than in the other tests, apparently because inelastic deflection was primarily in flexure. A joint-beam interface major flexural crack also significantly widened at -2.29% indicating bond-slip deformations. The peak strength was reached at -2.29% drift ($\gamma_j=8.2$). The first joint diagonal crack occurred at drift ratio of -5.5%. The inclination of main joint crack under downward loading was very steep, probably due to the high axial force. The main crack inclination was less steep under upward loading. The peak shear strain at joint strength under downward loading was -0.00009 radians, while that of upward loading was 0.016 radians. Axial failure took place at -7.71% drift, corresponding to axial load ratio of 0.47 and residual shear strength of 51%.

Table 3.1. Test results

Specimen ID	Beam	Direction	Displacement Ductility μ_d	Shear Failure			Axial Failure			
				Drift %	γ_j (psi ^{0.5})	$\frac{P}{f'_c A_j}$	Drift ratio %	Max. reached drift ratio %	$\frac{P}{f'_c A_j}$	γ_j (psi ^{0.5})
U-J-1	EW	Downward	4.89	-2.19	14.3	-0.31	-	-9.68	-	2.87
		Upward	3.42	3.42	10.9	0.09	-	9.68	-	-
	NS	Downward	3.33	-1.37	12.6	-0.30	-	-9.68	-	-
		Upward	2.87	2.19	9.6	0.05	-	9.68	-	-
U-J-2	EW	Downward	3.30	-1.30	9.98	-0.46	-	-3.42	-	4.30
		Upward	3.89	2.19	7.01	0.03	-	3.42	-	-
	NS	Downward	3.85	-0.82	8.97	-0.46	-	-2.19	-	-
		Upward	3.65	2.19	6.59	0.03	-	2.19	-	-
B-J-1	EW	Downward	3.00	-1.37	11.7	-0.45	-	-3.42	-	5.60
		Upward	1.90	2.19	10.1	0.01	-	3.42	-	-
	NS	Downward	2.90	-1.37	10.8	-0.45	-	-3.42	-	4.81
		Upward	2.28	2.19	9.83	0.01	-	3.42	-	-
U-BJ-1	EW	Downward	6.45	-2.29	8.20	-0.50	-	-7.71	-	4.19
		Upward	3.06	5.50	7.51	0.05	-	5.50	-	-
	NS	Downward	8.18	-2.29	7.38	-0.50	-	-5.50	-	-
		Upward	3.70	3.57	7.60	0.05	-	5.50	-	-

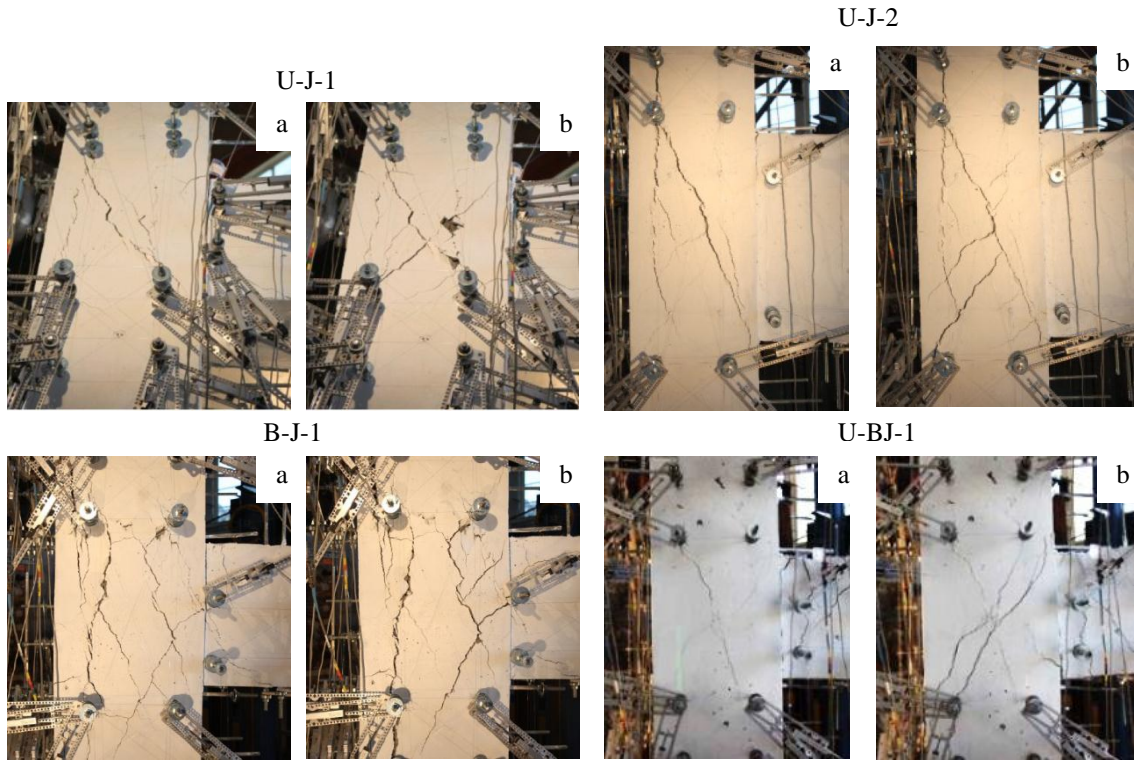


Figure 3.2. Shear failure of test specimen a) Downward loading b) Upward loading

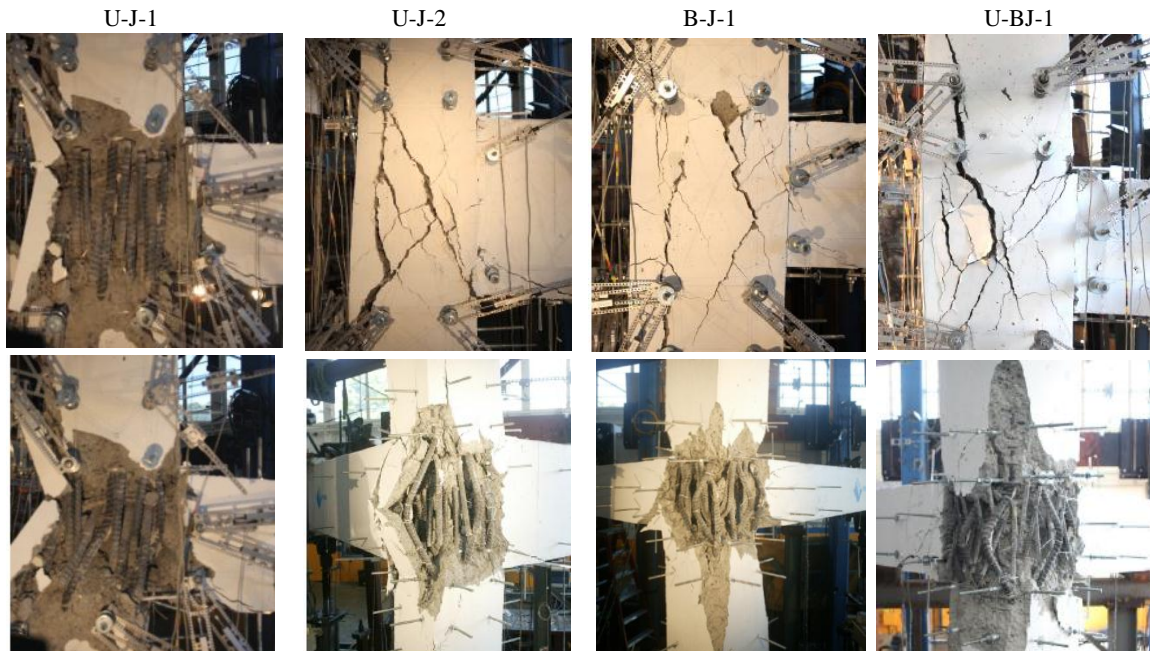


Figure 3.3. Test specimen axial failure mode, Top: at the onset of axial failure, Bottom: after axial failure

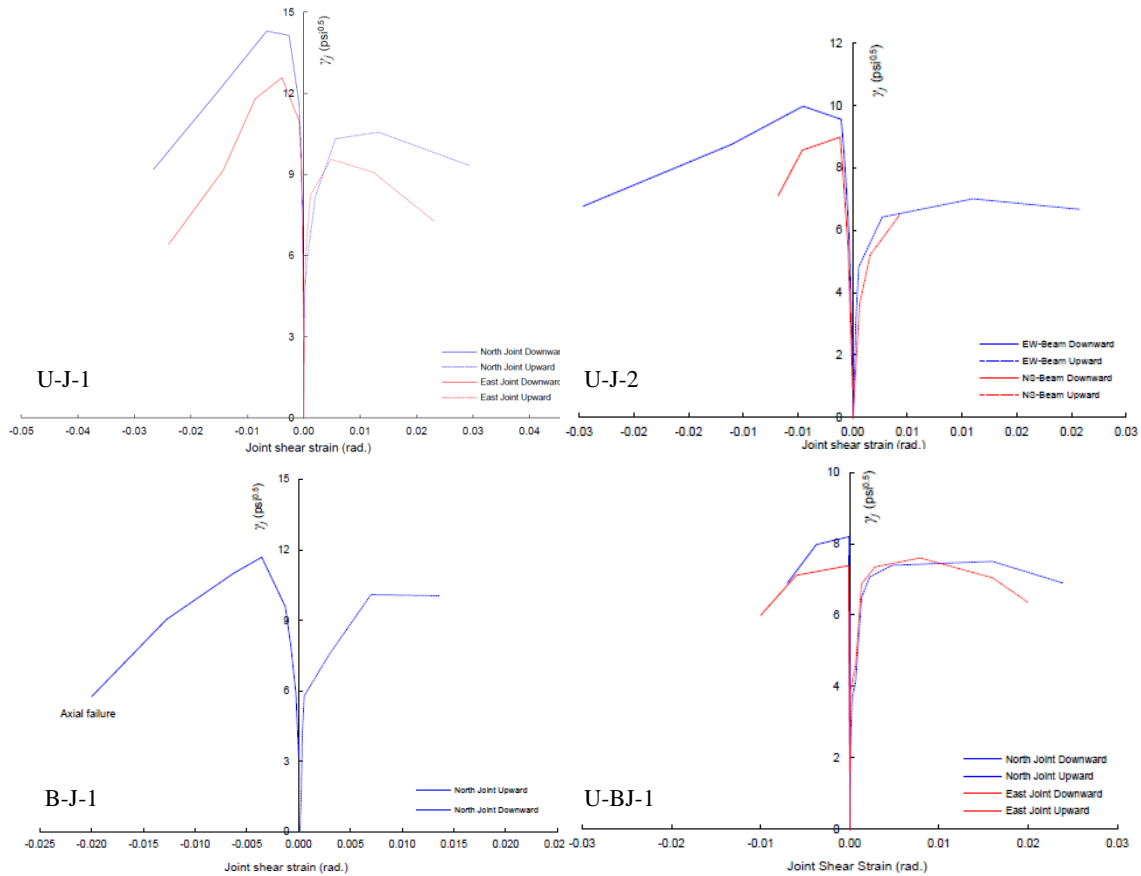


Figure 3.4. Joint shear stress-strain backbone curves of test specimens

4. EFFECT OF TEST PARAMETERS

4.1. Effect of Axial Load Ratio

Figure 4.1.a compares results obtained from two nominally identical test specimens sustaining J-Failure; Specimen U-J-2 was tested in the current test program with maximum axial load ratio of -0.46 for downward beam loading, and Specimen SP4 (Park, 2010) was tested in a companion test program with maximum axial load ratio of -0.15 for downward loading. Under higher axial load, U-J-2 was stiffer and sustained higher joint shear strength than SP4. The post-peak stiffness and strength degradation also were substantially accelerated in U-J-2 leading to axial failure at -3.06% drift, compared to -6.02% drift reached by SP4, at which the test was terminated without axial failure.

The effect of high axial load on BJ-Failure specimens was different. Figure 4.1.b plots the shear stress-drift backbone curve for specimen U-BJ-1, with peak strength axial load ratio of -0.5, compared to that of SP1 by Park 2010, with a -0.11 peak strength axial load ratio. The level of axial load did not affect joint shear strength in the case of BJ-Failure mode. This is because joint strength was controlled by beam flexural strength. Joint shear strains (not shown) were greatly reduced under high axial loads. It is speculated that higher axial load “clamped” beam longitudinal bar anchorages, decreasing strain penetration into the joint, and thereby reducing joint shear strength degradation. Consequently, specimens with higher axial load sustaining BJ-Failure may have overall higher deformation capacity.

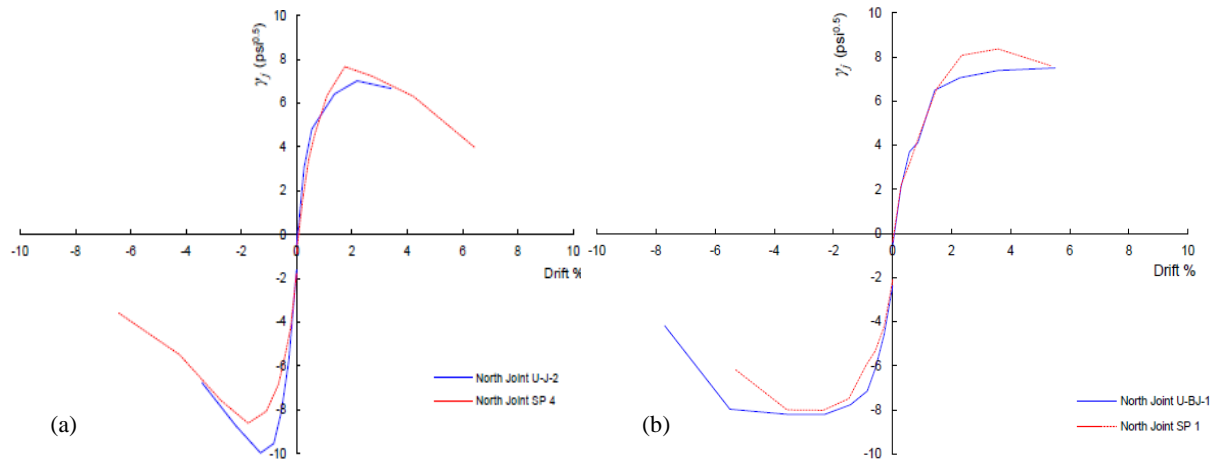


Figure 4.1. Effect of axial load level on shear stress-drift response of a) J-Failure joints, b) BJ-Failure joints

4.2. Effect of Joint Aspect Ratio

Figure 4.2.a compares the shear force-drift backbone relations of specimen U-J-1, with $\alpha_j=1$ and specimen SP4 (Park 2010) with $\alpha_j=1.67$, both with a comparable axial load levels. Joint shear strength is significantly reduced by increasing joint aspect ratio due to steeper joint strut inclination. The strut-tie-model and the empirical strength model proposed in Hassan 2011 were able to accurately model the effect of joint aspect ratio on joint strength. It is evident from Fig. 4.2.a that the aspect ratio had negligible effect on post-peak joint shear strength degradation.

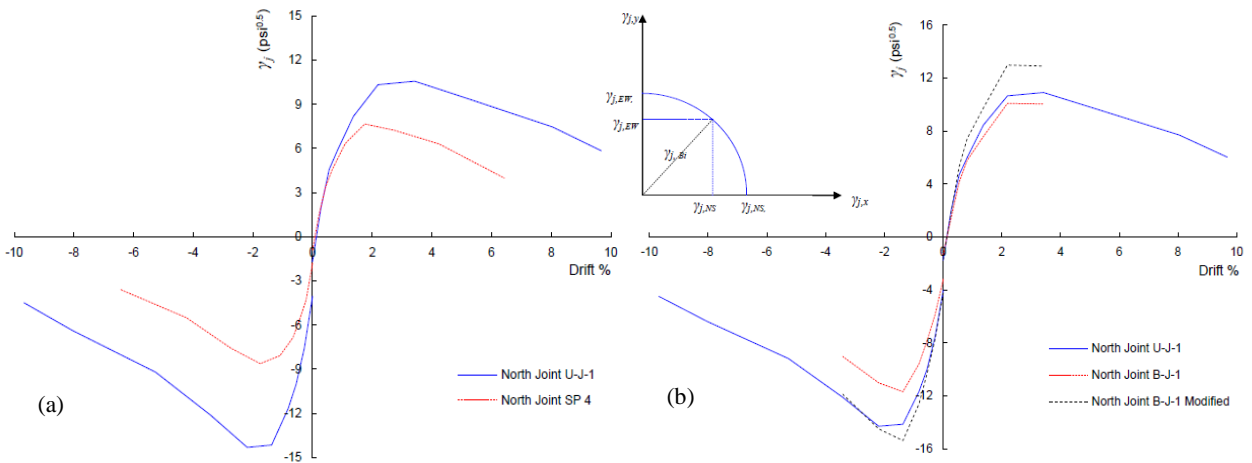


Figure 4.2. Effects of a) joint aspect ratio, b) loading history on shear stress-drift response of J-Failure joints

4.3. Effect of Loading History

Figure 4.2.b depicts the shear force-drift backbone for specimens U-J-1 and B-J-1, along with a modified B-J-1 response that incorporates an elliptical shear strength interaction to convert the orthogonal unidirectional shear of specimen B-J-1 to a bidirectional shear on a 45° angle. Shear strength along principal framing lines of a biaxially loaded joint was about 25% lower than that of uniaxially loaded joint for aspect ratio of 1 under compressive joint loading. However, biaxial shear strength along the biaxial lateral loading direction under compression loading was close to the shear strength of uniaxially loaded joints. This observation suggests that a circular (or perhaps elliptical) biaxial shear strength relation may

be appropriate to approximate strength of biaxially loaded joints. Drift ratio at peak shear strength was slightly reduced when applying the simultaneous biaxial loading. The higher flexibility of specimen B-J-1 is evident. This is partially due to the lower stiffness of the column. In addition, joint cracking started earlier, and stiffness degradation and post-peak pinching were more evident under bidirectional loading.

4.4. Effect of Beam Reinforcement Ratio

Joint shear strength is proportional to beam reinforcement within the BJ-Failure mode ratio until the threshold limit of J-Failure capacity (Hassan 2011). Within BJ-Failure, joint shear strength is essentially equal to shear stress demand from beam flexural capacity up to the limit of J-Failure strength. Beyond the J-Failure shear capacity, increasing beam reinforcement has no appreciable effect on shear strength.

5. CONCLUSIONS

A series of tests on corner beam-column, reinforced concrete joints without transverse reinforcement is reported. Two principal modes of failure were identified, J-Failure in which joint shear failure occurs without beam yielding and BJ-Failure in which joint shear failure occurs following beam yielding. In the latter case, joint shear strength is determined by beam flexural strength. In the former, joint strength depends on column axial force ratio, joint aspect ratio, and loading direction (uniaxial versus biaxial). Higher axial force decreases displacement ductility, drift capacity, and post-peak strength and stiffness of J-Failure joints. On the contrary, high axial force improves deformation capacity of joints controlled by BJ-Failure. This is due to the higher joint rigidity and the clamping action that delays yield penetration of beam longitudinal reinforcement within the joint. Increasing joint aspect ratio reduces shear strength of J-Failure joints. It seems that the elliptical interaction of joint shear strength is a good representation for bidirectional joint shear strength. Within the joint aspect ratios and reinforcement details tested, it appears that axial failure is not likely within the practical drift ratios of older concrete buildings. A 3% drift was achieved under axial load ratio of 0.46 and a joint aspect ratio of 1.67. However, larger joint aspect ratios and joints with different reinforcement detailing might be susceptible to axial failure at earlier drifts.

ACKNOWLEDGMENT

Financial assistance provided by U.S. National Science Foundation (NSF) award #0618804 through George E. Brown Jr. Network for Earthquake Engineering Simulation (NEES) and the Egyptian Department of Education award #2005292 through National Housing and Building Research Center is greatly appreciated.

REFERENCES

- ASCE/SEI 41-06. Seismic Rehabilitation of Existing Buildings. American Society of Civil Engineers. Virginia, USA
- Hassan, W. M. (2011). Analytical and Experimental Assessment of Seismic Vulnerability of Beam-Column Joints without Transverse Reinforcement in Concrete Buildings. PhD Dissertation, University of California, Berkeley, California, USA.
- Hassan, W. M., Park, S., Lopez, R., Mosalam, K. M., and Moehle, J. P. (2010). Seismic Response of Older-Type Reinforced Concrete Corner Joints. Proceedings, 9th U.S. National Conference and 10th Canadian Conference of Earthquake Engineering, Toronto, Canada, paper No. 1616.
- Park, S. (2010). Experimental and Analytical Studies on Old Reinforced Concrete Buildings with Seismically Vulnerable Beam-Column Joints. PhD Dissertation, University of California, Berkeley, USA.